Ostwald ripening of two-dimensional homoepitaxial islands

Frank Haußer* and Axel Voigt†
Crystal Growth Group, Research Center caesar, Ludwig-Erhard-Allee 2, 53175 Bonn, Germany
(Received 10 February 2005; revised manuscript received 18 April 2005; published 14 July 2005)

Ostwald ripening in homoepitaxy in the submonolayer regime is studied by means of numerical simulations based on a step flow model, which accounts for attachment-detachment kinetics at the island boundaries. Diffusion-limited ripening and the crossover to attachment-limited ripening is investigated. The simulations indicate that the coarsening kinetics of the average island radius is described by a t^a power law, where $1/3 \leqslant a \leqslant 1/2$. Here a takes the value $1/3$, if the ripening is purely diffusion-limited (infinite attachment rate at the island boundaries), and increases with decreasing attachment rate, approaching the value $a=1/2$ if the ripening becomes attachment-limited. For the diffusion-limited regime, the numerical simulations are shown to correspond with the predictions of the mean-field theory proposed by Yao *et al.*, for both the scaling behavior of the average island size as well as the island size distribution in the late stage. Approaching the attachment-limited regime, the numerical results meet the predictions of the classical mean-field theory of Lifshitz, Slyozov, and Wagner for attachment-limited ripening. We also analyze the influence of anisotropic edge energies and edge diffusion.

DOI: 10.1103/PhysRevB.72.035437 PACS number(s): 68.55.−a, 81.15.Aa

I. INTRODUCTION

In general, a two-phase mixture composed of a dispersed second phase in a matrix is not in thermodynamic equilibrium. The total energy of the two-phase system can be decreased via an increase in the size scale of the second phase, thus reducing the free energy associated with the interfaces between the two phases. If the second phase is present in the form of a distribution of clusters of different sizes, the large clusters grow at the expense of the small ones. This type of coarsening is known as Ostwald ripening.[1] The kinetics of Ostwald ripening is governed by two different processes:[2–4] the mass transport between the clusters via a diffusion field in the matrix and the attachment-detachment process at the cluster boundaries. Thus, two limiting kinetic regimes may be considered: in the *diffusion-limited* (DL) regime the attachment and detachment of particles at the cluster boundaries is fast compared to the diffusion in the matrix, thus diffusion is the limiting process; in the *attachment-limited* (AL) regime, the attachment and detachment at the cluster boundaries is slow compared to the diffusion in the matrix and therefore, in this case, attachment and detachment are the limiting processes.

In this paper we consider two-dimensional Ostwald ripening in homoepitaxy in the submonolayer regime (see Fig. 1). Here the minority phase (second phase) consists of atomic-height islands sitting on an atomically flat crystalline surface. Understanding the ripening of islands is clearly a necessary first step in gaining more insight into the more complicated processes in epitaxy, in particular the thermal decay of nanostructures. Moreover, with the advent of powerful experimental methods such as scanning tunneling microscopy (STM) and low-energy electron microscopy, it has become possible, to observe, *in situ*, the evolution of homoepitaxial islands during ripening. Comparing experimental results of the decay rates with theoretical model descriptions may even allow one to determine material parameters, which are difficult to obtain otherwise. STM measurements of island coarsening on TiN(001), TiN(111),[5] and on Cu(111) (Ref. 6) have been used to obtain step edge energies and activation barriers for attachment and detachment. In,[7] Ostwald ripening on Si(001) is demonstrated to be attachment-limited and also used to obtain adatom diffusion constants. The ripening of two-dimensional Ag islands on Ag(111) was investigated experimentally in Ref. 8, and also compared with numerical simulations based on a nearest-neighbor model, revealing that the ripening is clearly diffusion-limited. Because of the large variety of process conditions and materials grown by epitaxy, it may be assumed that also the intermediate regime, where attachment-detachment and diffusion are rate limiting, is of interest. However, as far as we know, there is no experimental investigation for this regime, presumably because

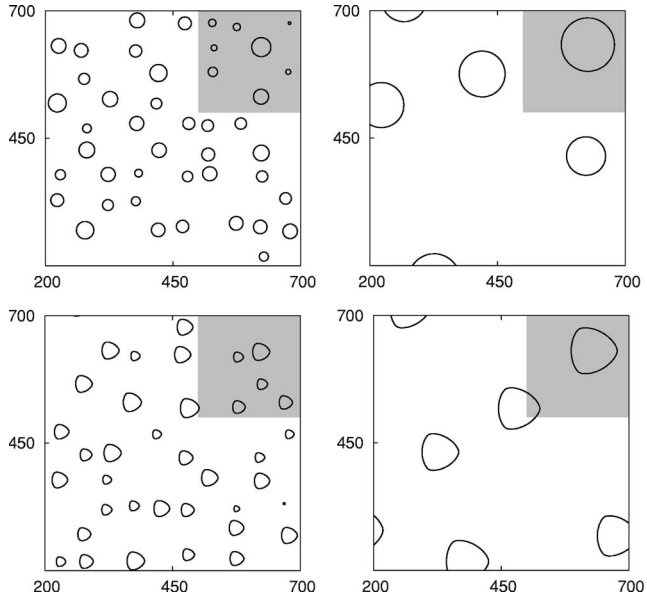

FIG. 1. Numerical simulation of two-dimensional Ostwald ripening with isotropic (top) and anisotropic (bottom) edge energy. Depicted are the island boundaries at times $t=600$ (left) and 15 000 s (right); length is measured in units of lattice spacing. A more detailed view of the shaded region is given in Fig. 8.

matching of experimental data to theoretical model parameters is rather involved in this case.

A major advance in the theoretical description of Ostwald ripening was made by Lifshitz, Slyozov, and Wagner (LSW).[2,3] Here, the ripening process is described in terms of a particle size distribution function of the second phase. The LSW theory predicts that the particle size distribution function asymptotically evolves to a unique form, being self-similar under scaling of the average particle size. Moreover, the average particle size asymptotically obeys a temporal power law. Both results are valid in the limit of vanishing volume fraction of the second phase. Meanwhile quite a few extensions of the LSW theory have been proposed, which take into account finite volume fractions; see, e.g., Refs. 9 and 10. For a review on theoretical work on Ostwald ripening we refer to Refs. 4 and 11.

The main part of the analytical work on Ostwald ripening is concerned with the three-dimensional diffusion-limited regime, usually in the context of binary alloys. Only a few investigations have been carried out on diffusion-limited ripening in two dimensions. A mean-field theory for finite coverage is derived, e.g., in Refs. 10, 12, and 13.

Most of the numerical simulations of Ostwald ripening are based on some approximations to circumvent the explicit solution of a moving-boundary problem for a large number of islands. Assuming the islands to be circular with immobile centers, the system is typically transformed into a dynamical system for the evolution of the island radii $R_i(t)$ (e.g., Ref. 10). Without relying on these assumptions, phase field models and boundary integral methods have been used to perform large scale simulations of two-dimensional Ostwald ripening for binary alloys (e.g., Refs. 14–17). A numerical simulation of Ostwald ripening in homoepitaxy has been presented in Ref. 18 using the level set method. In all cases, the diffusion-limited regime has been considered.

The goal of this work is to perform numerical simulations of the complete moving boundary problem related to homoepitaxy, allowing anisotropic edge energies and the investigation of the crossover from diffusion-limited to attachment-limited ripening. To our knowledge, neither theoretical nor numerical work exists on the crossover regime so far.

In Sec. II we briefly review the Burton-Cabrera-Frank (BCF) type model for step flow in epitaxy, which accounts for adatom diffusion, attachment-detachment kinetics at the island edges, and edge diffusion along the island edges. The crystal anisotropy enters through an anisotropic edge energy. The LSW analysis in the formulation of Wagner[3] is reviewed in Sec. III for the two limiting regimes (DL and AL). In Sec. IV, we present our numerical results. We start with investigating a four-island system in some detail. It is demonstrated how mean-field theories of the LSW type must fail due to local interactions of the islands. As expected, the importance of local interactions depends on the mass transport mechanism: being rather small in the AL regime it increases while approaching the DL regime. Next, results for large systems consisting of 400 islands are presented. For the DL regime, our simulation results confirm the predictions of the self-consistent mean-field theory proposed by Yao *et al.*[10] for both the scaling behavior of the average island size as well as the late-stage island size distribution. Our main results concern the crossover regime. The simulations indicate that the coarsening kinetics of the average island radius is described by a t^a power law, where $1/3 \leqslant a \leqslant 1/2$. Here a takes the value $1/3$, if the ripening is purely diffusion-limited, and increases with decreasing attachment rate—approaching the value $a=1/2$ if the ripening is purely attachment-limited. Moreover we find that the scaled island size distribution also evolves to a rather time-independent shape in the mixed regime.

II. STEP FLOW MODEL

We briefly review the BCF-type step flow model, as described in more detail, e.g., in Refs. 19 and 20. Let $\Omega \subset \mathbb{R}^2$ be the substrate with $\Omega_i \subset \Omega$, $i=0, 1$ denoting the region of atomic height i (we only consider the submonolayer regime) and $\Gamma = \bar{\Omega}_0 \cap \bar{\Omega}_1$ the island boundaries. Thus the minority phase is represented by the monolayer islands Ω_1. Denote by $\rho_i = \rho_i(x,t)$ the adatom density on terrace $\Omega_i(t)$ $(i=0, 1)$ at time t. The adatom diffusion on a terrace is described by the diffusion equation for the adatom density

$$\partial_t \rho_i - \vec{\nabla} \cdot (D \vec{\nabla} \rho_i) = 0 \quad \text{in } \Omega_i(t), \tag{1}$$

where $D>0$ is the surface diffusivity. Note that we have neglected desorption. Throughout the paper the unit of length will be the substrate lattice spacing a. Thus the adatom density ρ denotes the number of adatoms per adsorption site. Now let j^+, j^- be the normal adatom flux at the boundary Γ from the upper and lower terraces, respectively, which are given by

$$j^+ := -D \vec{\nabla} \rho_1 \cdot \vec{n} - v \rho_1,$$

$$j^- := D \vec{\nabla} \rho_0 \cdot \vec{n} + v \rho_0, \tag{2}$$

where $\vec{n}$ and v are the unit normal pointing from the upper to the lower terrace and the normal velocity of the step $\Gamma(t)$, respectively, with the convention that $v>0$, if the movement of $\Gamma(t)$ is in the direction of $\vec{n}$. Assuming first-order kinetics for the attachment and detachment at the island boundaries ("reaction kinetics"), the adatom density satisfies the following kinetic boundary conditions at the island boundaries $\Gamma(t)$:

$$j^+ = k_+(\rho_1 - \rho_{eq}), \quad j^- = k_-(\rho_0 - \rho_{eq}), \tag{3}$$

where ρ_{eq} is the equilibrium density at $\Gamma(t)$. With this notation $0<k_+<k_-$ models the Ehrlich-Schwoebel effect.[21] Moreover, if $k_+, k_- \to \infty$, Eqs. (3) pass into the thermodynamic boundary condition $\rho_1 = \rho_0 = \rho_{eq}$ at $\Gamma(t)$. Within this limit, the island boundaries act as perfect sinks for the adatom density and the growth and shrinking of islands is purely diffusion-limited.

The equilibrium adatom density ρ_{eq} is described by the Gibbs-Thomson-type relation[19,20]

$$\rho_{eq} = \rho^*(1 + \tilde{\gamma}\kappa), \quad \tilde{\gamma}(\theta) = \gamma(\theta) + \gamma_{\theta\theta}(\theta), \tag{4}$$

where γ denotes the orientation-dependent step free energy divided by $k_B T$, κ is the curvature of the boundary $\Gamma(t)$, and

θ is the angle between the outer normal and the x axis.

For the motion of the steps, we assume the following law for the normal velocity v of the island boundaries $\Gamma(t)$:

$$v = j^+ + j^- + \partial_s[\nu\partial_s(\tilde{\gamma}\kappa)], \tag{5}$$

where ν and ∂_s denote the mobility of the edge diffusion and the tangential derivative along the steps, respectively. The last term in Eq. (5) represents step edge diffusion of edge adatoms along the steps, whereas the first two terms ensure the adatom mass conservation.

III. TWO-DIMENSIONAL LSW ANALYSIS

In this section we will review the LSW analysis in the formulation of Wagner.[3] The results for two-dimensional systems are somewhat spread, with regard to the literature. So it seems to be worthwhile to give a common treatment of the diffusion-limited and attachment-limited ripening adapted to the step flow model as described in Sec. II. We will primarily follow the exposition given in Ref. 4. Being aware of the limitations of the Wagner analysis it still offers a very compact formulation and is therefore chosen here to derive the theoretical scaling laws and size distribution functions in the limit of vanishing coverage (area fraction). The two-dimensional attachment-limited case has been treated in a similar fashion in Ref. 22. The diffusion-limited case is treated in Refs. 10 and 12, where a mean-field theory for finite coverage is developed and the LSW distribution is obtained in the limit of vanishing coverage. Both derivations rely on a cutoff of the diffusion field at some *ad hoc* chosen distance from the island to circumvent the difficulties arising from the logarithmic singularities of the fundamental solution for a single island in two dimensions. Here, however, we will use an argument given (and also derived rigorously) in Ref. 23, which allows the direct use of the Wagner analysis as in the three-dimensional case.

The first basic assumption of the LSW theory is that the coverage ϕ (area fraction) of the second phase is very small. Hence, in the notation given in Sec. II, the region Ω_1 consists of many disconnected islands far away from each other. Moreover, the islands are assumed to be radially symmetric with immobile centers. Thus the morphology of the dispersed spherical second phase may be characterized in terms of an island radius distribution function $F(R,t)$. The number of islands per unit area is then given by $n(t)=\int_0^\infty F(R,t)dR$. Assuming that no nucleation and coalescence of islands takes place, F obeys the continuity equation

$$\partial_t F + \partial_R(\dot{R}F) = 0. \tag{6}$$

The flux of islands in size space is controlled by the function $\dot{R}(R)$. This function embodies much of the physics of the ripening problem, and must therefore be carefully constructed.

Since in epitaxy the diffusion constant is very large, we may pass to the quasistationary approximation, i.e., we neglect the time derivative in Eq. (1) and the convective terms in Eqs. (2). Moreover, we assume isotropic edge energies. The edge diffusion term in Eq. (5) vanishes since all islands are assumed to be circular. We also assume for simplicity that there is no Ehrlich-Schwoebel barrier, i.e., $k:=k_+=k_-$. Passing to the excess density $u:=\rho-\rho^*$, Eqs. (1)–(5) become

$$\Delta u_i = 0 \quad \text{in } \Omega_i, \quad i=0,1, \tag{7}$$

$$-D\vec{\nabla}u_1\cdot\vec{n} = k(u_1-\rho^*\tilde{\gamma}\kappa) \quad \text{on } \Gamma, \tag{8}$$

$$D\vec{\nabla}u_0\cdot\vec{n} = k(u_0-\rho^*\tilde{\gamma}\kappa) \quad \text{on } \Gamma, \tag{9}$$

$$v = D(\vec{\nabla}u_1-\vec{\nabla}u_0)\cdot\vec{n} \quad \text{on } \Gamma. \tag{10}$$

To obtain an explicit solution for $\dot{R}(R)$ from the above model, LSW make the following second assumption: Far away from the islands, the excess density u may be approximated by a spatially constant mean field $\bar{u}(t)$. Under these assumptions, the growth rate of an island is determined by the growth rate of an isolated island obeying Eqs. (7)–(10) supplemented by the boundary condition

$$u_0(\infty,t) = \bar{u}. \tag{11}$$

However, in contrast to the three-dimensional case, Eq. (11) does not lead to a solution of the system (7)–(10) due to the logarithmic divergence of the fundamental solution of Eq. (7). Following Ref. 23, we introduce the typical island distance d, the typical island radius R, and assume $R \ll d$ such that $\phi:=\pi(R/d)^2$ is the coverage. Now consider an island of radius R centered at the origin. Equation (11) is substituted by

$$u_0(d,t) = \bar{u}. \tag{12}$$

Equations (7)–(10) may then be solved explicitly and the growth rate of a single island is obtained as

$$\dot{R}(t) = \frac{\rho^*\tilde{\gamma}}{R}\left(\frac{R}{R_c}-1\right)\frac{kD}{D+kR\ln(1/\phi^{1/2})}. \tag{13}$$

Here the critical radius R_c of an island that neither grows nor shrinks is given in terms of the mean field $\bar{u}$ as

$$R_c = \rho^*\tilde{\gamma}/\bar{u}.$$

In view of Eq. (13), the dimensionless parameter

$$\alpha := \frac{D}{\bar{R}k\ln(1/\phi^{1/2})} \tag{14}$$

(where $\bar{R}$ denotes the average island radius) describes to what extent the mass transport is diffusion or attachment dominated: $\alpha \ll 1$ and $\alpha \gg 1$ correspond to the DL and the AL regime, respectively. For the two limiting cases, Eq. (13) may be substituted by either

$$\dot{R}(t) = K_{DL}\frac{1}{R^2}\left(\frac{R}{R_c}-1\right), \quad K_{DL} = \frac{D\rho^*\tilde{\gamma}}{\ln(1/\phi^{1/2})} \tag{15}$$

for DL ripening or

$$\dot{R}(t) = K_{AL}\frac{1}{R}\left(\frac{R}{R_c} - 1\right), \quad K_{AL} = k\rho^* \tilde{\gamma} \tag{16}$$

for AL ripening. Proceeding in the spirit of Wagner[3] as described in Ref. 4, one introduces the new variables

$$z = \frac{R}{R_c}, \quad \tau = \ln\left(\frac{R_c(t)}{R_c(0)}\right). \tag{17}$$

Equations (15) and (16) become

$$\frac{dz}{d\tau} = \nu\frac{z-1}{z^\lambda} - z, \tag{18}$$

where $\lambda = 2$ (DL) or 1 (AL) and

$$\nu = \frac{K_{DL/AL}}{R_c^2 \dot{R}_c(t)}. \tag{19}$$

The continuity equation (6) for $f(z,\tau) := F(R_c z, t(\tau))R_c$ is given in the new coordinates as

$$\partial_\tau f + \partial_z\left(\frac{dz}{d\tau} f\right) = 0. \tag{20}$$

Moreover, following Wagner, we make the simplifying assumption that the coverage ϕ is a conserved quantity at late times, which yields the following mass conservation constraint:

$$\phi = \pi R_c^2 \int_0^\infty z^2 f(z,\tau) dz \quad \text{for } \tau \text{ large}. \tag{21}$$

To find a unique solution $f(z,\tau)$ of Eqs. (18)–(21), the essential point of the LSW analysis is to argue that ν becomes constant and takes a unique value at late times (i.e., $\tau \to \infty$), which in turn implies a scaling law for the critical radius R_c by solving the ordinary differential equations (ODEs) for $R_c(t)$ given in Eq. (19). To argue that ν is asymptotically constant, Eq. (20) is solved by a separation ansatz

$$f(z,\tau) = g(\tau)h(z). \tag{22}$$

First, the continuity equation (20) implies that the temporal decrease of the number of islands is given by the islands with a (scaled) radius approaching $z=0$, i.e.,

$$\frac{d}{d\tau}\int_0^\infty f(z,\tau) dz = \lim_{z\to 0}\left(\frac{dz}{d\tau} f\right). \tag{23}$$

Now note that, for $z \ll 1$, Eq. (18) becomes

$$\frac{dz}{d\tau} = -\frac{\nu}{z^\lambda}. \tag{24}$$

Plugging Eq. (24) into Eq. (23) and using the ansatz (22), we obtain

$$\frac{dg}{d\tau}\int_0^\infty h(z) dz = -g(\tau)\nu \lim_{z\to 0}[z^{-\lambda} h(z)]. \tag{25}$$

Thus, assuming the decrease of the number of islands per unit area to be finite and positive, $h(z)$ has to be of the form $h(z) = h_0 z^\lambda + O(z^3)$, for $z \ll 1$, for some constant h_0 and therefore Eq. (25) becomes

$$\frac{dg}{d\tau}\frac{1}{g(\tau)} = -\frac{\nu h_0}{\int h(z) dz}. \tag{26}$$

To show that the left-hand side of Eq. (26) is a constant—which in turn implies that ν does not depend on τ and is therefore also constant—the separation ansatz (22) is plugged into the mass conservation constraint (21) to obtain

$$g(\tau) = \frac{\phi}{\pi R_c^2 \int z^2 h(z) dz}. \tag{27}$$

Using $dR_c/d\tau = R_c$, this implies

$$\frac{dg}{d\tau}\frac{1}{g(\tau)} = -\frac{2}{R_c}\frac{dR_c}{d\tau} = -2, \tag{28}$$

and therefore ν is constant.

Now the continuity equation (20) may be integrated straightforwardly using the separation ansatz (22). One obtains

$$g(\tau) \sim \exp(-2\tau) \sim R_c^{-2}, \tag{29}$$

$$h(z) = h_0\left(\frac{dz}{d\tau}\right)^{-1} \exp\left[\int\left(\frac{dz}{d\tau}\right)^{-1}\right]. \tag{30}$$

To explicitly calculate the function $h(z)$ from Eq. (30), the final step of the Wagner analysis consists in claiming that a cutoff value z_0 exists [i.e., $h(z)=0$ for $z \geqslant z_0$] and uniquely determining z_0 and the value of ν in the coarsening rate (18). Instead of repeating the partly heuristic arguments of Wagner, we quote some arguments taken from Refs. 4 and 22 by examining how the function $dz/d\tau$ varies with z and τ. As depicted in Fig. 2, four qualitatively different cases may be distinguished. For negative ν values the relative growth rate is positive for small relative island radii z and negative for bigger ones, which is clearly opposite to the real physical process. Now, if ν is positive, $dz/d\tau$ generally has a maximum and can have two zeros on the x axis. In the case of two zeros, $z_1 < z_2$, islands with a relative radius z such that $z_1 < z < z_2$ would grow until $z = z_2$ and islands bigger than z_2 would shrink until $z = z_2$, i.e., we would end with an ensemble of islands having the identical radius $z = z_2$, which would be stable against coarsening, in contradiction to thermodynamics. If $dz/d\tau$ has no intercept with the x axis, all islands would have a negative growth rate and thus all islands would finally disappear. There is exactly one value of ν such that only the islands with a specific relative radius $z =: z_{max}$ have a zero growth rate, which occurs if the maximum of $dz/d\tau$ touches the x axis. Choosing this value for ν and a cutoff value z_0 of $h(z)$ as $z_0 = z_{max}$ yields a physical reasonable process. These considerations uniquely fix the values of both ν and z_0 to be

$$z_0 = 3/2, \quad \nu = 27/4 \quad \text{(DL)},$$

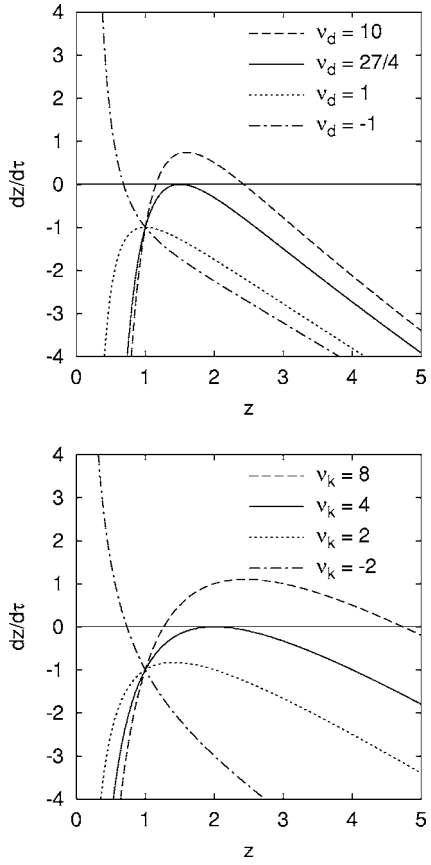

FIG. 2. Dependence of $dz/d\tau$ on ν: DL (top); AL (bottom).

$$z_0 = 2, \quad \nu = 4 \quad \text{(AL)}.$$

Having fixed the value of ν, the spatial distribution function $h(z)$ may be calculated explicitly from Eqs. (18) and (30). Normalizing $h(z)$, one obtains the *scaled normalized island size distribution functions* $h_{DL}(z)$ (DL)[10,13] and h_{AL} (AL):[22]

$$h_{DL}(z) = \begin{cases} 72e^{2/3}z^2(z+3)^{-17/9}(2z-3)^{-28/9}\exp\left(\dfrac{-2}{3-2z}\right), & z \leqslant \dfrac{3}{2}, \\ 0, & z > \dfrac{3}{2}, \end{cases} \tag{31}$$

$$h_{AL}(z) = \begin{cases} 8e^2 z(2-z)^{-4}\exp\left(\dfrac{-4}{2-z}\right), & z \leqslant 2, \\ 0, & z > 2. \end{cases} \tag{32}$$

To compare with numerical simulations, it is more convenient to express $h(z)$ in terms of the variable $r = R/\bar{R}$, i.e. (see Fig. 3),

$$H(r) := z_{av} h(z_{av} r) \quad \text{where } z_{av} = \int_0^\infty z h(z) dz. \tag{33}$$

The temporal scaling law for the critical island radius R_c is obtained by integrating Eq. (19) as

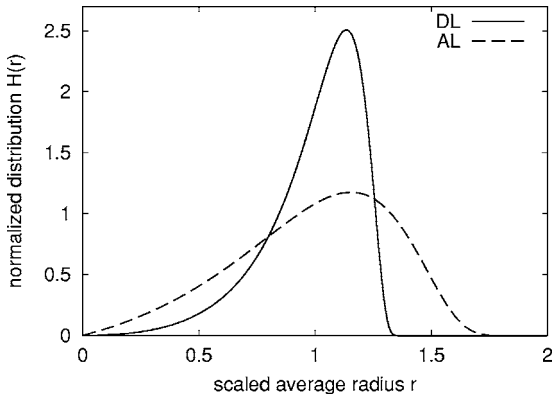

FIG. 3. LSW normalized scaled island size distribution function $H(r)$ as defined in Eq. (33); diffusion-limited (DL, solid) and attachment-limited (AL, dashed).

$$R_c(t) = \begin{cases} \left(R_c(0)^3 + \dfrac{4}{9}\dfrac{D\rho^* \tilde{\gamma}}{\ln(1/\phi^{1/2})} t \right)^{1/3} & \text{(DL)} \\ \left(R_c(0)^2 + \dfrac{1}{2} k \rho^* \tilde{\gamma} t \right)^{1/2} & \text{(AL)}. \end{cases} \tag{34}$$

We finally note that $\bar{R} = R_c$ for AL, whereas $\bar{R} = 1.0665 R_c$ for DL.

One should be aware that the above results are valid only in the limit of vanishing coverage ϕ and at late times. The Wagner analysis has been criticized since it is not self-consistent due to the assumption of a constant coverage [see Eq. (21)]. Indeed, in a self-consistent treatment the mean field $\bar{u}$ has to be determined by the mass conservation constraint

$$\bar{u}(t) + \pi \int_0^\infty R^2 f(R,t) dR = \text{const}.$$

Using a different approach, Marqusee and Ross[9,24] showed, that the assumption of a fixed coverage ϕ is not necessary for the derivation of a temporal scaling law and self-similar distribution function. Moreover they demonstrate that the effect of changes of the coverage does not alter the zeroth-order result but enters only in the first- and higher-order corrections in ϕ. Note that the LSW analysis is a one-particle approximation since the growth rate of a particle does only depend on its size, which is not true for finite coverage ϕ. Quite a few mean-field theories have been proposed, which account for finite coverage.[9,10,12] Most of them are concerned with three-dimensional ripening and all of them treat the diffusion-limited case. These theories predict a temporal scaling law of the form $\bar{R}(t) = [\bar{R}(0)^3 + K(\phi)t]^{1/3}$, where the coarsening rate $K(\phi)$ increases with increasing coverage ϕ. Moreover, all of them obtain a time-independent scaled island size distribution, which in general broadens with increasing coverage. However, the values of $K(\phi)$ and the specific form of the distribution function differ considerably in these theories.

IV. NUMERICAL RESULTS

In this section, we present numerical results for systems with finite coverage. Since we numerically solve the complete two-dimensional free boundary problem given in Eqs. (1)–(5), we are not restricted to any of the idealizing assumptions of the previous section. Thus it will be possible to investigate the influence of edge diffusion and anisotropic edge energies, and the effect of finite coverage. Moreover, we do not have to stick to either the diffusion-limited or the attachment-limited regime, but may also explore the intermediate regime.

The numerical method is based on adaptive finite elements, and Eqs. (1)–(5) are discretized using an operator splitting approach: We use two independent numerical grids: a two-dimensional grid for the adatom diffusion on the terraces and a one-dimensional grid for the evolution of the island boundaries. In each time step: (i) we update the discrete step boundaries by solving a geometric partial differential equation based on the adatom densities and the discrete island boundaries from the previous time step; (ii) we solve the diffusion equation to update the adatom densities using the adatom densities from the previous time step and the computed discrete representation of the island boundaries. Adaptivity in space and time is indispensable for this approach to be efficient, especially if long-time behavior, as in Ostwald ripening, is considered. For a detailed description of the algorithm see Refs. 25 and 26.

A. Four-island system

To investigate the influence of nearest-neighbor islands in more detail, we simulated the ripening of four islands on a periodic domain of size 100×100, varying the attachment rate k while keeping all other parameters constant. The initial configuration is depicted in Fig. 5 (top). The two smallest islands of type 1 are closer to island 2 than to island 3, where island 2 is smaller than island 3. Note that the coverage is very small ($\phi\approx0.008$). Let us first analyze what the classical LSW theory predicts: As has been noted above, the classical LSW theory is a *one-particle approximation*, i.e., islands of the same size are shrinking or growing with the same velocity depending only on the mean field or equivalently the critical radius $R_c(t)$ [see Eqs. (15) and (16)]. Assuming conservation of the total island area as in Eq. (21), i.e., $(d/dt)\Sigma_i R_i^2=0$, yields

$$R_c=\left(\frac{1}{N}\sum_i\frac{1}{R_i}\right)^{-1}\quad\text{(DL)},\quad R_c=\frac{1}{N}\sum_i R_i\quad\text{(AL)},\quad(35)$$

where the sum is taken over all islands with positive radius $R_i>0$ and N is the number of islands with $R_i>0$. Also note that in the DL regime, the mean field becomes singular, whenever an island disappears. Figure 4 presents a numerical simulation of the ripening of four islands until the first two islands have disappeared, using the dynamical system given by Eqs. (15), (16), and (35).

There are two reasons why a mean-field picture may fail for finite coverages: first neighboring islands may shadow the diffusion field ("screening") and second the diffusion is not infinitely fast. In both cases, the ripening of an individual island depends not only on the mean field generated by the whole ensemble of islands but on the local gradient of the adatom density, where the latter depends on the local environment. In most experimental situations in epitaxy, the first influence does not play an important role, since the "diffusion length" $l_*=\sqrt{Dt_*}$, where t_* is the distinction time of a typical island in the experiment, is much larger than the sample length.[7] For all parameters used in the simulations in this section $l_*>2.5\times10^3$, which is much larger than the sample size. Figure 5 depicts the results of the numerical simulation of the complete moving boundary problem Eqs. (1)–(5) for different values of the attachment rate k (while leaving all other parameters constant). The qualitative behavior dramatically depends on the extent to which the ripening is diffusion-limited (left) or attachment-limited (right). In the DL case, one observes that despite island 2 being initially smaller than island 3, it grows faster than island 3. This becomes even more apparent in Fig. 6 (left): the area lines cross, which is in clear contradiction to the prediction of any mean-field theory. In contrast, in the case of AL ripening [see Fig. 5 (right)], the system behaves as predicted by the LSW theory [compare Figs. 4 and 6 (left)]. As already mentioned above, the variation of the gradient of the diffusion field is much larger in the DL regime, whereas the diffusion field approaches a constant (apart from the discontinuity at the island boundaries) in the attachment-limit. This is confirmed in Fig. 5 (bottom), where the diffusion field on half of the domain is depicted for the DL (left) and AL (right) regimes at time $t=0$.

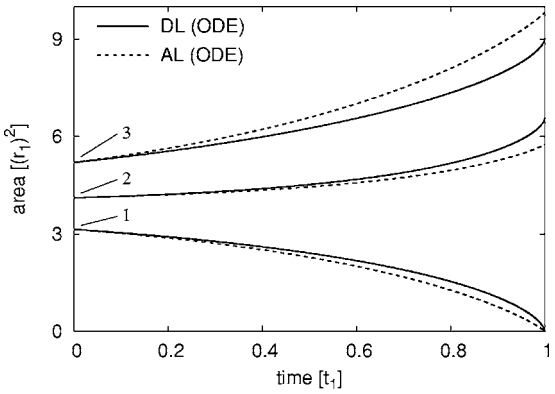

FIG. 4. Ripening of four islands with radii $r_1=7$, $r_2=8$, $r_3=9$ on a periodic domain of size 100×100 as assumed by the classical LSW theory: numerical solution of the dynamical system given in Eqs. (15), (16), and (35). Time is measured in units of the distinction time t_1 of the two smallest islands with radius r_1. The initial configuration is as in Fig. 5.

To investigate the influence of an anisotropic edge energy γ, we perform the same simulations but chose an anisotropic stiffness of the form

$$\tilde{\gamma}(\theta)=\{a^2\sin^2[\phi(\theta)]+b^2\cos^2[\phi(\theta)]\}^{3/2},$$

$$\phi(\theta)=\tan^{-1}\left(\tan(\theta+\pi/2)\frac{b}{a}\right).\quad(36)$$

This stiffness yields an ellipsoid with aspect ratio a/b as equilibrium shape, where we have chosen $a/b=2.5$. This

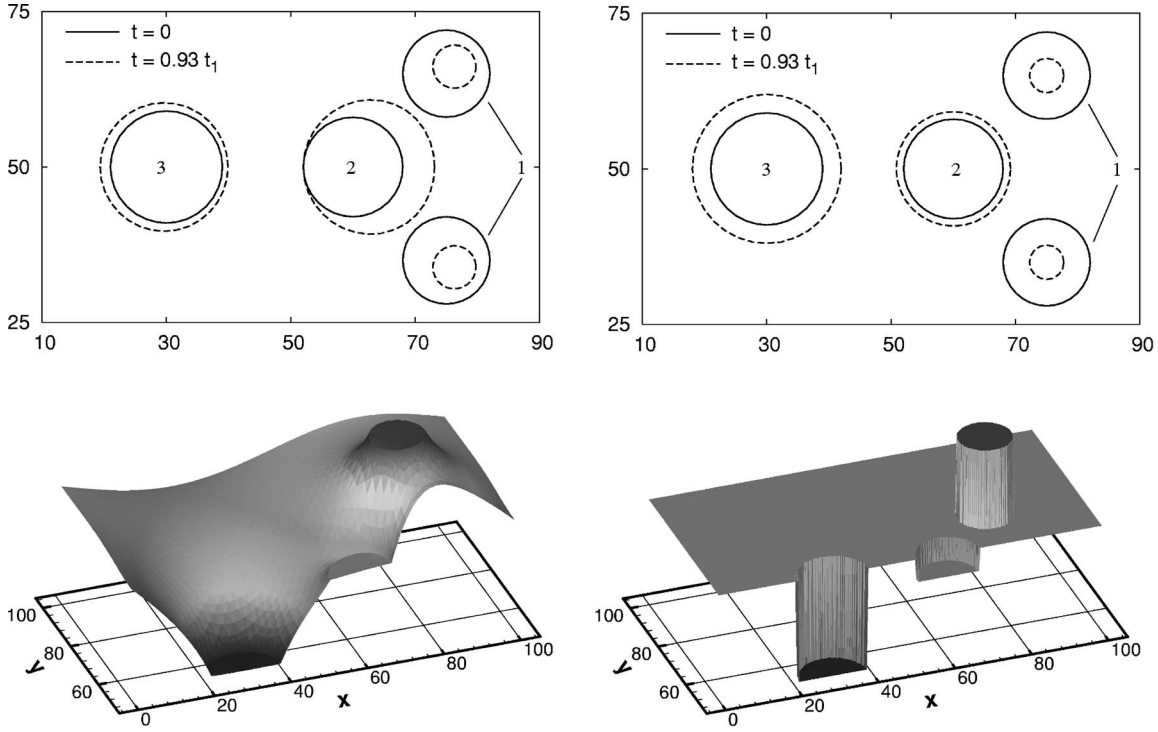

FIG. 5. Ripening of four islands with radii $r_1=7$, $r_2=8$, $r_3=9$ on a periodic domain of size 100×100. Time is measured in units of the distinction time t_1 of the two smallest islands of type 1. (Top left) For diffusion-limited ripening ($D/k=0$) one observes that despite island 2 being initially smaller than island 3, it grows faster than island 3. The reason for this is a strong screening effect: island 2 grows at the expense of the two islands of type 1, while shadowing island 3. (Top right) In the attachment-limited regime ($D/k=1.4\times10^3 r_1$), the screening effect vanishes. The bottom row depicts the adatom density ρ at $t=0$ for the diffusion-limited (left) and the attachment-limited (right) regime. As can be seen, the adatom density varies strongly in the DL case, whereas it becomes nearly constant in the AL case (apart from the discontinuity at the island boundaries). Thus in the latter case the assumption of a constant mean-field $\bar{\rho}$ at some distance of the islands is much more appropriate.

choice of anisotropy is motivated by Ref. 7, where Ostwald ripening of ellipsoidal silicon islands on Si(001) has been investigated. As depicted in Fig. 7, the qualitative behavior is as in the isotropic case. This indicates that anisotropy of the edge energy does not play an important role in Ostwald ripening. This will also be confirmed in the large-scale simulations below.

B. Island movement, anisotropic edge energy, and edge diffusion

Now, the initial setup is as follows: 400 islands are placed on a 1000×1000 periodic domain. To avoid overlapping, the midpoints of the islands are placed on a regular grid and are then shifted randomly. The radii of the islands are chosen randomly according to the diffusion-limited LSW distribution as given in Eq. (33) (see also Fig. 3). Finally, the islands are projected onto the Wulff shape (with the same area) corresponding to the anisotropic edge energy. If not otherwise stated, the following parameters are used:

$$D=10^5, \quad \rho^*=10^{-4}, \quad \nu=0.0, \quad \gamma(\theta)=1.0.$$

If anisotropy is taken into account, we use the anisotropic edge energy

$$\gamma(\theta)=1.0+0.1\cos(3\theta). \tag{37}$$

To investigate the influence of edge diffusion, we have compared simulations with the same initial configuration but choosing the edge diffusion mobility ν to be either 0.0 or 1.0. For isotropic as well as anisotropic edge energy of the form given in Eq. (37), there is no influence of edge diffusion seen in the simulations. That is, the island shapes retain the Wulff shape during coarsening, also without edge diffusion. This is different in the growth regime, where at least some deviation from the Wulff shape is observed and the island shape stays closer to the Wulff shape, if edge diffusion is included (see Ref. 26). Consequently there is also no influence on the scaling behavior and the island size distribution function. Therefore in the following we will always neglect edge diffusion, i.e., we chose $\nu=0.0$. Certainly, edge diffusion does play a significant role in the high-coverage regime, where coalescence of islands takes place. We would like to note that for a more realistic simulation of Ostwald ripening in the presence of a crystal anisotropy, one would also have to consider anisotropic adatom diffusion and anisotropic edge diffusion, which may be built into the numerical algorithm easily.

To demonstrate the influence of the local environment once again, some stages of ripening with isotropic and with anisotropic edge energy are depicted in Fig. 8, which is an enlargement of Fig. 1. The assumption of mean-field theories that the centers of the islands are fixed can clearly be seen to

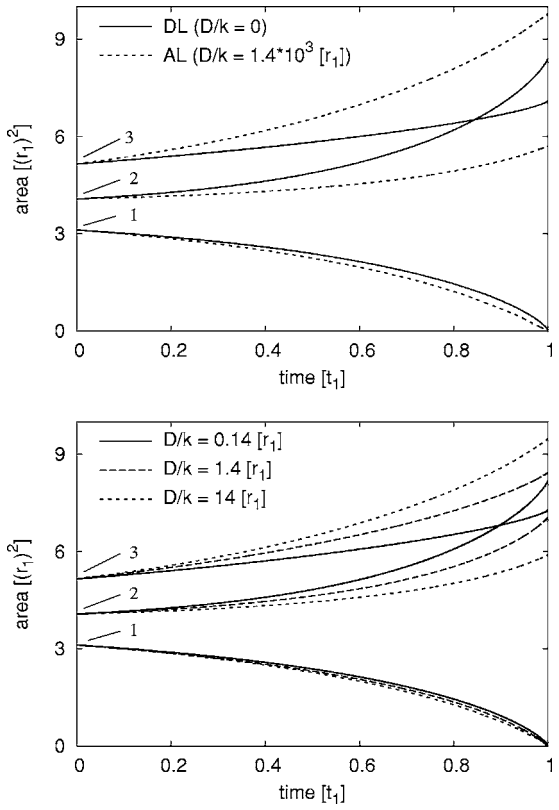

FIG. 6. Ripening of four islands with initial configuration as in Fig. 5: Area versus time until the two smallest islands have vanished. Time is measured in units of the distinction time t_1 of the two smallest islands of type 1 and length in units of the island radius r_1. In the upper figure the two limiting cases are considered. Note that the AL case is well described by the LSW dynamics (compare Fig. 4), while the DL case shows a crossing of the area decay lines, which clearly manifests the influence of the local environment and thus the breakdown of the mean-field picture. The lower figure shows the crossover regime from AL to DL.

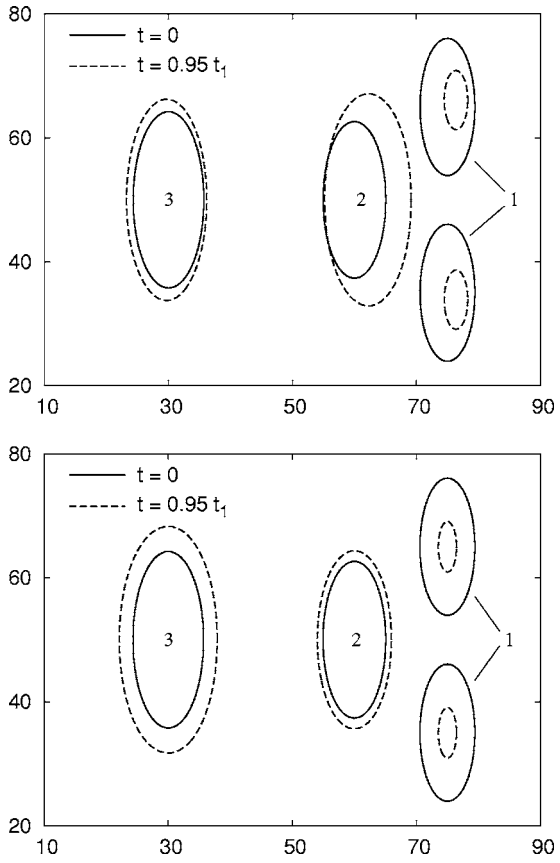

FIG. 7. Ripening of four islands with same areas as in Fig. 5, but anisotropic stiffness $\tilde{\gamma}$ as given in Eq. (36) (i.e., the equilibrium shape is an ellipsoid with aspect ratio 2.5). Here t_1 denotes the distinction time of the two smallest islands of type 1. As in the isotropic case, the DL regime (top) shows a strong screening effect as opposed to the AL regime (bottom), leading to a crossing of the area decay lines as in Fig. 6.

be not satisfied. Also, the ripening of an individual island depends strongly on the surrounding islands.

C. Scaling of the average island size

To determine the scaling exponent for diffusion-limited ripening in the late stage, a log-log plot of the average island radius versus time is presented in Fig. 9. Here the number of islands decreases from 400 to 50. For each value of the coverage ϕ, the results of five simulations with different randomly chosen initial configurations have been averaged. An affine linear fit of the data yields the scaling exponents. The values for the exponents are 0.332 and 0.325 for coverages $\phi=0.085$ and 0.01, respectively, and correspond well with the theoretical value of $1/3$. We would like to remark that the number of islands is reduced by one-eighth in the simulations, which corresponds to a simulation time $\tau=3$ on the self-similar time scale. Thus any comparison with the asymptotic results of a mean-field theory has to be taken with some care and is a bit speculative.

Assuming a temporal power law for the average island radius $\bar{R}(t)$ of the form

$$\bar{R}(t) = [\bar{R}(0)^3 + K(\phi)t]^{1/3},$$

the coarsening rate $K(\phi)$ is determined as shown in Fig. 10 by an affine linear fit of the numerical data yielding $K(0.01)=2.6$ and $K(0.085)=4.4$, which seem to be in reasonable agreement with the predicted values given in Refs. 10 [Fig. 8(b)] and 12 (Fig. 2). [For a comparison note that with our parameters $D\rho^*\tilde{\gamma}=10$ in Eq. (34).]

Numerical results of the evolution of the average island size in the intermediate regime and the crossover to the attachment-limited regime are depicted in Fig. 11. The log-log plot of the average radius versus time indicates a temporal power law for the average island radius $\bar{R}$ in the late stage, i.e.,

$$\bar{R} \sim t^a, \tag{38}$$

where (for fixed coverage ϕ) a is a monotonically increasing function of α interpolating the diffusion-limited regime ($\alpha=0$, $a=1/3$) and the attachment-limited regime ($\alpha=\infty$, $a=1/2$). This is a quite remarkable result, which is clearly valid only for finite systems and finite time, since for an infinite system, the asymptotic regime should always become

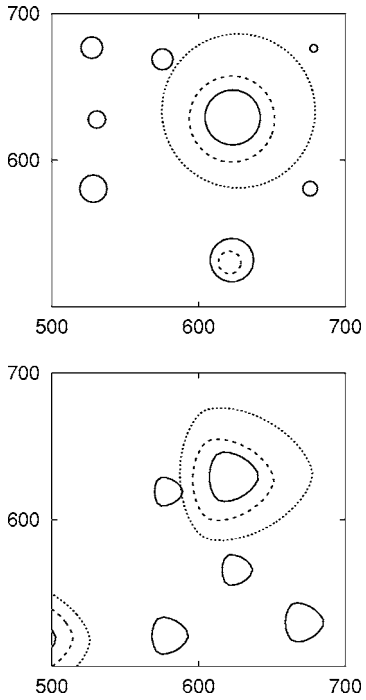

FIG. 8. Movement of islands during ripening: Island boundaries at $t=600$ (solid), 3000 (dashed), and 15 000 (dotted) for isotropic (top) and anisotropic (bottom) edge energy. Depicted is an enlargement of Fig. 1. The coverage is $\phi=0.085$ and the ripening is in the intermediate regime [$\alpha=2.7$ as given in Eq. (14)].

diffusion-limited due to the fact that $\bar{R}\to\infty$ and therefore $\alpha\to 0$ for $t\to\infty$. We also note that for the largest value $\alpha=37$ in the simulations, the coarsening exponent $a=0.48$ is in good agreement with the predicted value $a=0.5$ of the LSW theory for AL ripening.

D. Island size distribution function

We begin with investigating the diffusion-limited regime: The initial setup is chosen as in Sec. IV B. In particular, the initial random island size distribution is chosen according to

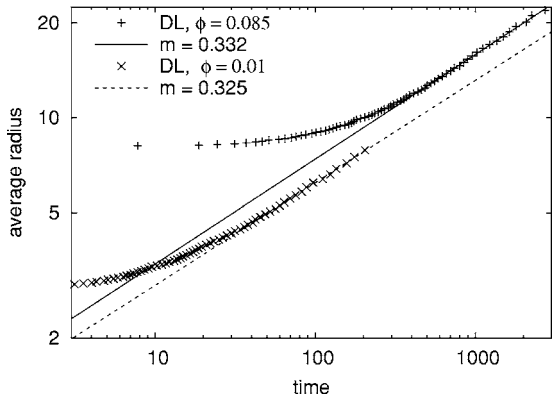

FIG. 9. Diffusion-limited ripening: log-log plot of the average radius $\bar{R}$ versus time for coverages $\phi=0.085$ and 0.01. The scaling exponent is determined by an affine linear fit in the late stage as 0.332 for $\phi=0.085$ (solid line) and 0.325 for $\phi=0.01$.

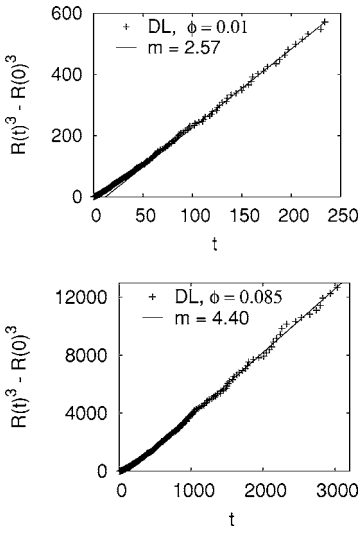

FIG. 10. Diffusion-limited ripening: Time evolution of the average island radius $\bar{R}(t)$. The plot of the numerical results for both coverages $\phi=0.01$ (top) and 0.085 (bottom) indicates that the average radius $\bar{R}(t)$ obeys the temporal scaling law $\bar{R}(t)^3=\bar{R}(0)^3+K(\phi)t$. The coarsening rate $m=K(\phi)$ is obtained by an affine linear fit, and the values are similar to the theoretical results of Refs. 10 and 12.

the DL LSW distribution as depicted in Fig. 3. Mean-field theories for finite coverages in the DL regime (see, e.g., Refs. 10 and 12) predict that the scaled distribution function broadens until it reaches an asymptotic time-independent shape, where the asymptotic distribution becomes broader with increasing coverage. In Fig. 12 the scaled normalized island size distribution in the late stage of the numerical simulations is depicted for two different coverages $\phi=0.01$ and 0.05. As demonstrated with level set simulations in Ref. 18, our numerical results are in good agreement with the asymptotic distribution predicted by the self-consistent mean-field theory of Yao *et al.*[10] Next, we turn to the crossover regime

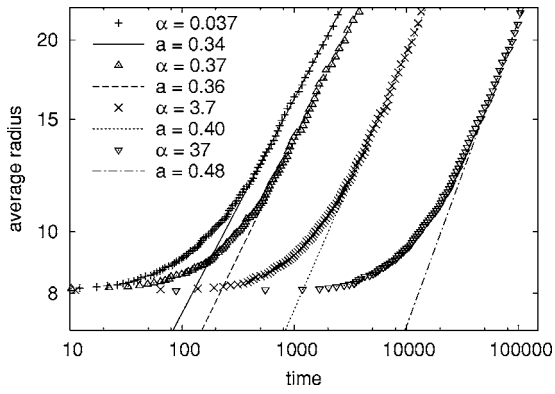

FIG. 11. Scaling of the average island radius $\bar{R}$: Crossover from diffusion- to attachment- limited ripening ($\alpha\ll 1$ to $\alpha\gg 1$). The scaling exponent a in Eq. (38) for different values of α is obtained by an affine linear fit of the log-log plot (average radius versus time) of the numerical data in the late stage. Here α is given in Eq. (14), with average radius $\bar{R}\approx 22$ taken at the end of the simulations, where the number of remaining islands is $N=50$.

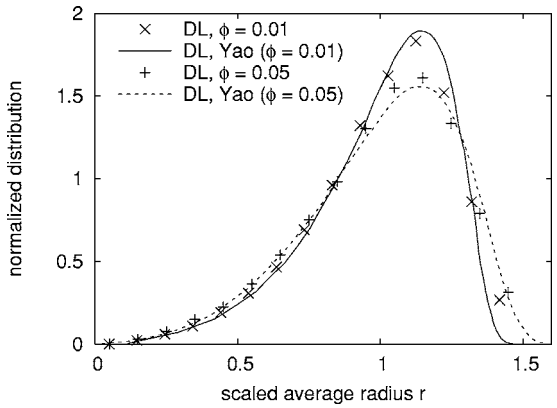

FIG. 12. Scaled normalized island size distribution for DL ripening in the late stage. The numerical data have been averaged for five different initial configurations randomly chosen according to the DL LSW distribution, and over the distributions from $N=100$ to 50 (N being the number of remaining islands), to get a good statistic. We note that in all cases the distributions stop broadening at least after $N=200$. The solid and dashed lines are the asymptotic distributions for $\phi=0.01$ and 0.05, respectively, as predicted by the mean-field theory of Yao *et al.* and are taken from Ref. 10, Fig. 10.

from DL to AL ripening: by varying the attachment rate k, with all other parameters fixed, the value of α as given in Eq. (14) varies from $\alpha=0$ to 72. As shown in Fig. 13, the late-stage distribution function broadens with increasing α, becoming very close to the AL LSW distribution, if $\alpha \gg 1$. Note, that we started with the very peaked DL LSW distribution. To demonstrate that the initial distribution has a minor influence on the late-stage distribution, simulations for $\alpha=37$ and $\phi=0.05$ but with different initial conditions have been performed: the first set of random initial distribution has been chosen according to the DL LSW distribution and the second set to the AL LSW distribution (see Fig. 3). The results of the numerical simulations are presented in Fig. 14. In both cases, the late stage is very close to the AL LSW distribution.

Concluding, there are two reasons that cause a broadening of the late-stage island size distribution function (as compared to the DL LSW distribution): The distribution becomes broader with increasing coverage and with increasing α, i.e., on crossing from the DL to the AL regime.

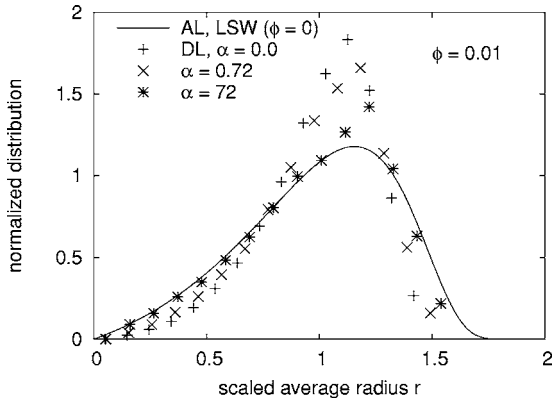

FIG. 13. Scaled normalized island size distribution function in the late stage: Crossover from DL to AL ripening. It is clearly seen, that the distribution function broadens with decreasing attachment rate, and becomes very close to the AL LSW distribution of Fig. 3, if $\alpha \gg 1$.

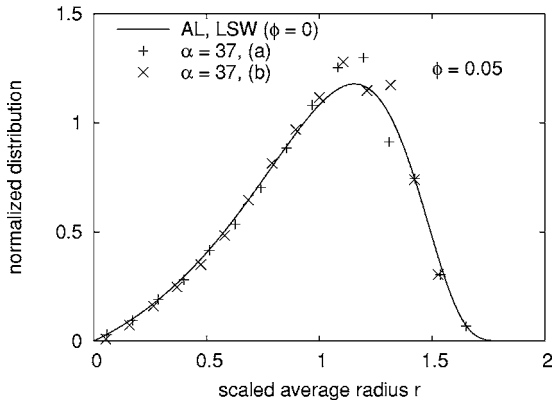

FIG. 14. Island size distribution function (AL): late-stage island size distribution, for two different initial distributions. (a) DL and (b) AL LSW distribution. In both cases, the late stage is very close to the AL LSW distribution.

V. CONCLUSIONS AND OUTLOOK

Using the numerical method as developed in Refs. 25 and 26, it is possible to perform numerical simulations of the step flow model describing homoepitaxial Ostwald ripening, without any simplifying assumptions. Anisotropic edge energies as well as edge diffusion may be incorporated. Most important, the attachment-detachment kinetics at the step edges is included. Thus it is possible, to investigate the crossover regime from diffusion-limited to attachment-limited ripening by numerical simulations.

Simulations of the ripening of a four-island system already reveal the breakdown of the mean-field approach concerning the prediction of the decay of a single island in the ensemble, as known from experiments.[7,8] This is due to the influence of the local environment, which cannot be captured by a mean-field approach. This becomes most pronounced in the DL regime, whereas the local environment becomes less important when approaching the AL regime, due to the fact that in the first case the adatom density near the island boundary (or equivalently, the local chemical potential) depends very much on the local environment, whereas in the latter case, the adatom density on the lower terrace approaches a constant value even near the island boundaries.

However, concerning scaling properties and asymptotic island size distributions, predictions of a mean-field theory may be very accurate. In particular we have found the predictions of a self-consistent mean-field theory proposed by Yao *et al.*[10] to correspond well to the numerical simulations of the complete model in the DL regime. Moreover, predictions of the classical LSW theory for AL ripening, concerning the scaling exponent of the average island size and the asymptotic island size distribution are in agreement with our simulations when approaching the AL regime.

Our main results concern the crossover regime. The simu-

lations indicate, that the coarsening kinetics of the average island radius is described by a t^a power law, where $1/3 \leqslant a \leqslant 1/2$. Here a takes the value $a=1/3$, if the ripening is purely diffusion-limited and increases with decreasing attachment rate–approaching $a=1/2$, if the ripening becomes attachment-limited. Certainly this is valid only for systems of medium size and finite times (i.e., this is not an asymptotic result), since for a very large (infinite) system, the asymptotic regime should always become diffusion-limited due to the fact that the average radius $\bar{R} \to \infty$ for $t \to \infty$. Moreover, the scaled island size distribution also becomes rather time independent in the late-stage. The late-stage distribution becomes broader when approaching the AL regime, and seems to converge to the AL LSW distribution. In conclusion, the reason for broadening of the asymptotic scaled island size distribution (as compared to the DL LSW distribution) seen in experiments may either be an increasing coverage ϕ or an increasing value of the parameter α, given in Eq. (14), which describes the crossover from the DL regime ($\alpha \ll 1$) to the AL regime ($\alpha \gg 1$). We finally note that a comparison of experiments and simulations in this crossover have not yet been carried out, but seems to be a promising way to determine material parameters such as attachment rates.

*Electronic address: Frank.Hausser@caesar.de
†Electronic address: Axel.Voigt@caesar.de

[1] W. Ostwald, Z. Phys. Chem., Stoechiom. Verwandtschaftsl. **34**, 495 (1900).
[2] I. M. Lifshitz and V. V. Slyozov, J. Phys. Chem. Solids **19**, 35 (1961).
[3] C. Wagner, Z. Elektrochem. **65**, 581 (1961).
[4] L. Ratke and P. W. Voorhees, *Growth and Coarsening: Ripening in Material Processing* (Springer, Berlin, 2002).
[5] S. Kodambaka, V. Petrova, A. Vailionis, P. Desjardins, D. Cahill, I. Petrov, and J. Greene, Thin Solid Films **392**, 164 (2001).
[6] G. Schulze Icking-Konert, M. Giesen, and H. Ibach, Surf. Sci. **398**, 37 (1998).
[7] N. C. Bartelt, W. Theis, and R. M. Tromp, Phys. Rev. B **54**, 11741 (1996).
[8] K. Morgenstern, G. Rosenfeld, and G. Comsa, Surf. Sci. **441**, 289 (1999).
[9] J. A. Marqusee and J. Ross, J. Chem. Phys. **80**, 536 (1984).
[10] J. H. Yao, K. R. Elder, and M. G. H. Guo, Phys. Rev. B **47**, 14110 (1993).
[11] P. W. Voorhees, J. Stat. Phys. **38**, 231 (1985).
[12] J. A. Marqusee and J. Ross, J. Chem. Phys. **81**, 976 (1984).
[13] T. M. Rogers and R. C. Desai, Phys. Rev. B **39**, 11956 (1989).
[14] N. Akaiwa and D. I. Meiron, Phys. Rev. E **51**, 5408 (1995).
[15] H. Garcke, B. Niethammer, M. Rumpf, and U. Weikard, Acta Mater. **51**, 2823 (2003).
[16] K. Thornton, N. Akaiwa, and P. W. Voorhees, Acta Mater. **52**, 1353 (2004).
[17] K. Thornton, N. Akaiwa, and P. W. Voorhees, Acta Mater. **52**, 1364 (2004).
[18] M. Petersen, A. Zangwill, and C. Ratsch, Surf. Sci. **536**, 55 (2003).
[19] P. Politi, G. Grenet, A. Marty, A. Ponchet, and J. Villain, Phys. Rep. **324**, 271 (2000).
[20] J. Krug, in *Multiscale Modeling of Epitaxial Growth*, edited by A. Voigt, ISNM Vol. 149 (Birkhäuser, Basel, 2005), p. 69.
[21] R. L. Schwoebel, J. Appl. Phys. **40**, 614 (1969).
[22] M. Hillert, Acta Metall. **13**, 227 (1965).
[23] B. Niethammer and F. Otto, Commun. Pure Appl. Math. **54**, 361 (2001).
[24] J. A. Marqusee and J. Ross, J. Chem. Phys. **79**, 373 (1983).
[25] E. Bänsch, F. Haußer, O. Lakkis, B. Li, and A. Voigt, J. Comput. Phys. **194**, 409 (2004).
[26] E. Bänsch, F. Haußer, and A. Voigt, SIAM J. Sci. Comput. (USA) (to be published).